PHYSICAL REVIEW B **96**, 100406(R) (2017)

Direct observation of magnon-phonon coupling in yttrium iron garnet

Haoran Man,[1] Zhong Shi,[2,3] Guangyong Xu,[4] Yadong Xu,[2] Xi Chen,[5] Sean Sullivan,[5] Jianshi Zhou,[5] Ke Xia,[6] Jing Shi,[2,*] and Pengcheng Dai[1,6,†]

[1]*Department of Physics and Astronomy, Rice University, Houston, Texas 77005, USA*
[2]*Department of Physics and Astronomy, University of California, Riverside, California 92521, USA*
[3]*School of Physics Science and Engineering, Tongji University, Shanghai 200092, China*
[4]*NIST Center for Neutron Research, National Institute of Standards and Technology, Gaithersburg, Maryland 20899, USA*
[5]*Materials Science and Engineering Program, Texas Materials Institute, The University of Texas at Austin, Austin, Texas 78712, USA*
[6]*Department of Physics, Beijing Normal University, Beijing 100875, China*

(Received 6 June 2017; revised manuscript received 12 August 2017; published 27 September 2017)

The magnetic insulator yttrium iron garnet (YIG) with a ferrimagnetic transition temperature of ∼560 K has been widely used in microwave and spintronic devices. Anomalous features in spin Seeback effect (SSE) voltages have been observed in Pt/YIG and attributed to magnon-phonon coupling. Here, we use inelastic neutron scattering to map out low-energy spin waves and acoustic phonons of YIG at 100 K as a function of increasing magnetic field. By comparing the zero and 9.1 T data, we find that instead of splitting and opening up gaps at the spin wave and acoustic phonon dispersion intersecting points, magnon-phonon coupling in YIG enhances the hybridized scattering intensity. These results are different from expectations of conventional spin-lattice coupling, calling for different paradigms to understand the scattering process of magnon-phonon interactions and the resulting magnon polarons.

DOI: 10.1103/PhysRevB.96.100406

Spin waves (magnons) and phonons are propagating disturbances of the ordered magnetic moment and lattice vibrations, respectively. They constitute two fundamental quasiparticles in a solid and can couple together to form a hybrid quasiparticle [1,2]. Since our current understandings of these quasiparticles are based on linearized models that ignore all high-order terms than the quadratic terms and neglect interactions among the quasiparticles themselves [3], magnons and phonons are believed to be stable and unlikely to interact and break down for most purposes [4]. Therefore, discovering and understanding how otherwise stable magnons and phonons can couple and interact with each other to influence the electronic properties of solids are one of the central themes in modern condensed matter physics.

In general, spin-lattice (magnon-phonon) coupling can modify magnons in two different ways. First, a static lattice distortion induced by the magnetic order may affect the anisotropy of magnon exchange couplings, as seen in the spin waves of iron pnictides with large in-plane magnetic exchange anisotropy [5]. Second, dynamic lattice vibrations interacting with time-dependent spin waves may give rise to significant magnon-phonon coupling [6,7]. One possible consequence of such coupling is to create energy gaps in the magnon dispersion at the nominal intersections of magnon and phonon modes [8,9], as seen in the antiferromagnet $(Y,Lu)MnO_3$ [10]. Alternatively, magnon-phonon coupling may give rise to spin-wave broadening at the magnon-phonon crossing points [11]. In both cases, we expect the integrated intensity of hybridized excitations at the intersecting points to be the sum of separate magnon and phonon scattering intensities without spin-lattice coupling [8]. Finally, if the magnon and phonon lifetime broadening is smaller than their interaction strength, the resulting mixed quasiparticles can form magnon polarons [6,7].

Here, we use inelastic neutron scattering to study low-energy ferromagnetic magnons and acoustic phonons in the ferrimagnetic insulator yttrium iron garnet (YIG) with a chemical formula $Y_3Fe_5O_{12}$ [Figs. 1(a)–1(d)] [12–14]. At zero field and 100 K, we confirm the quadratic wave-vector dependence of the magnon energy $E = Dq^2$, where D is the effective spin-wave stiffness constant and q is momentum transfer (in $Å^{-1}$ or 10^{10} m^{-1}) away from a Bragg peak [Fig. 1(e)] [13–19]. We also confirm the linear dispersion of the transverse acoustic (TA) phonon mode [Fig. 1(e)]. Upon application of a magnetic field H_0, a spin gap of magnitude gH_0 ($g \approx 2$ is the Landé electron spin g-factor) opens and lifts up the spin-wave spectra away from the field-independent phonon dispersion [Figs. 1(f) and 1(g)] [13,14]. By comparing the 0 and 9.1 T field wave-vector dependence of the spin-wave spectra, we find that instead of splitting and opening up gaps at the spin wave and acoustic phonon dispersion intersecting points, hybridized magnon polaron scattering at the intersecting points has a larger intensity at zero field and magnons remain unchanged at other wave vectors, as shown schematically in the bottom panels of Figs. 1(f) and 1(g). This is different from the expectations of conventional magnon-phonon interactions, where hybridized polaronic excitations at the crossing points should have the sum of separate magnon and phonon scattering intensities, and become broader in energy due to repulsive magnon-phonon dispersion curves [8–11]. Our results thus reveal a different magnon-phonon coupling mechanism, calling for another paradigm to understand the scattering process of magnon-phonon interactions and the resulting magnon polarons [20].

We chose to study magnon-phonon coupling in YIG because it is arguably the most important material used in microwave and recent spintronic devices [21]. In addition to having a ferrimagnetic ordering temperature of ∼560 K

*jings@ucr.edu
†pdai@rice.edu

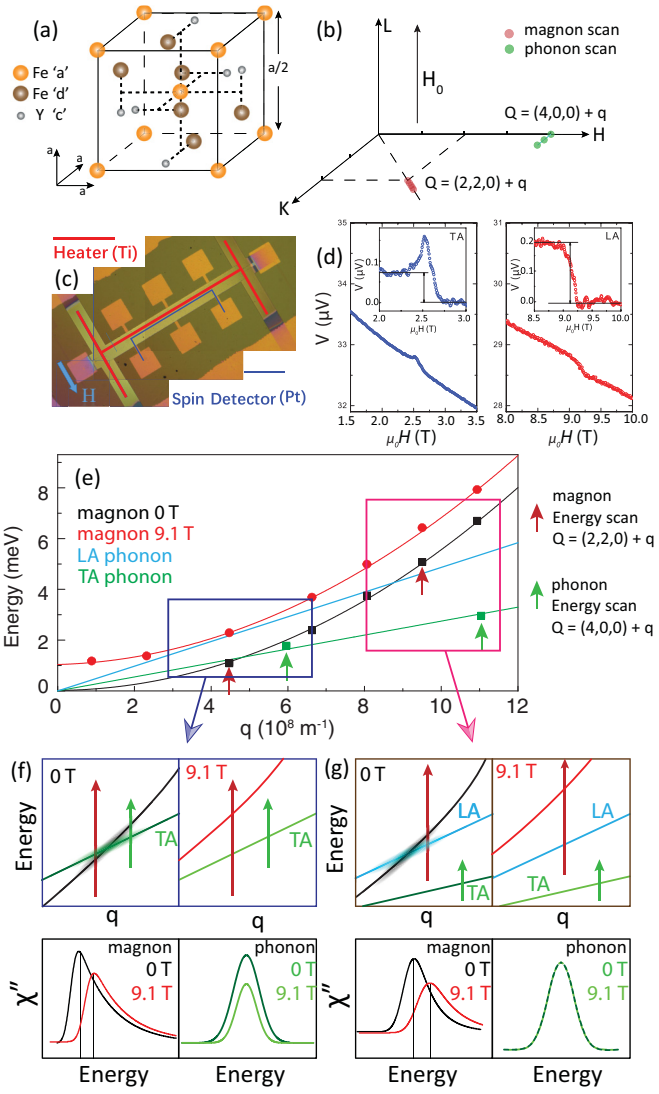

FIG. 1. (a) The full unit cell of YIG comprises eight cubes that are related by glide planes to the basic cube shown in the figure. (b) Corresponding reciprocal space with $[H,K,0]$ scattering and vertical magnetic field H_0. The red and green solid circles mark the positions of reciprocal space where we probe spin waves and acoustic phonons, respectively. (c) A picture of the Pt/YIG device used for SSE measurements. (d) SSE voltage in the field ranges where anomalous features appear at 100 K. (e) Magnon and phonon dispersions of YIG at 100 K and different magnetic fields. The black squares and solid red circles are data from 0 and 9.1 T measurements, respectively. The $q \approx 4.5 \times 10^8$ m^{-1} point corresponds to $\Delta Q = 0.062$ in Fig. 2(d). The black and red solid lines are quadratic ferromagnetic spin waves fit to the data. The blue and red boxes indicate magnon-phonon crossing points. The green and blue solid lines are the TA (with phonon velocity $C_\perp \approx 3.9 \times 10^3$ m/s) and LA ($C_{||} \approx 7.2 \times 10^3$ m/s) phonons, respectively [20]. (f), (g) Expanded view of the blue and red boxes in (e), respectively. The bottom panels in (f) and (g) summarize the results obtained in our measurements on the magnetic field effect on spin waves, hybridized excitations, and TA phonons.

suitable for room-temperature applications, YIG can be grown with an exceptional quality, and has the lowest Gilbert damping of any known materials and a narrow magnetic resonance linewidth allowing for the transmission of spin waves over macroscopic distances [22–24]. The spin Seebeck effect (SSE), which allows spin currents produced by thermal gradients in magnetic materials to be transmitted and converted to charge voltages in a heavy metal such as Pt, is one of the most technologically relevant thermoelectric phenomena to be used in "spin caloritronic" devices [25–36]. In the case of a Pt film on the surface of a polished single-crystalline YIG slab (Pt/YIG) [Fig. 1(c)] [31], anomalous features in the magnetic field dependence of SSE voltages at low temperatures are attributed to the magnon-phonon interaction at the "touching" points between the magnon and transverse acoustic (TA) and longitudinal acoustic (LA) phonons as the magnon dispersion curve is lifted by the applied field while the phonon is not affected by the field [Fig. 1(d)] [20]. While we find no anomaly at the magnon and TA/LA acoustic phonon touching points, our data reveal clear evidence for magnon-phonon interactions at zero field, consistent with the formation of magnon polarons.

Our neutron scattering experiment was carried out at NIST Center for Neutron Research, Gaithersburg, Maryland [32]. The full body-centered-cubic unit cell of YIG with space group $Ia3d$ comprises eight cubes that are related by glide planes to the basic cube, as shown in Fig. 1(a), where the metallic atomic sites are labeled as a, d, and c [13]. Using the cubic lattice parameter of $a = b = c = 12.376$ Å, we define momentum transfer $\mathbf{Q}$ in three-dimensional (3D) reciprocal space in Å^{-1} as $\mathbf{Q} = H\mathbf{a}^* + K\mathbf{b}^* + L\mathbf{c}^*$, where H, K, and L are Miller indices and $\mathbf{a}^* = \hat{\mathbf{a}}2\pi/a$, $\mathbf{b}^* = \hat{\mathbf{b}}2\pi/a$, $\mathbf{c}^* = \hat{\mathbf{c}}2\pi/a$ [Figs. 1(a) and 1(b)]. Consistent with Ref. [20], the magnetic field dependence of SSE voltage on our Pt film on YIG contains two anomalous features at 2.5 and 9.1 T [Figs. 1(c)–1(e)] [32].

The sample for neutron scattering experiments was oriented with the a and $b(a)$ axis of the crystal in the horizontal $[H,K,0]$ scattering plane [Fig. 1(b)] and mounted inside a 10 T vertical field magnet. In this geometry, we measured magnon dispersion around (2,2,0) and phonon dispersion around (4,0,0). The momentum transfers $\mathbf{Q}$ at these wave vectors are $\mathbf{Q}_{\text{magnon}} = (2 + \Delta Q, 2 + \Delta Q, 0)$ and $\mathbf{Q}_{\text{phonon}} = (4, \Delta Q, 0)$ for the TA phonon [Fig. 1(b)]. For convenience, we calculate the relative momentum transfer as $q = 2\pi\sqrt{2}\Delta Q/a$ for magnons and $q = 2\pi\Delta Q/a$ for phonons. We chose (2,2,0) for magnetic and (4,0,0) for phonon measurements because of their huge differences in nuclear structure factors [4.75 at (2,2,0) vs 50.5 at (4,0,0)], which are directly related to the acoustic phonon intensity. Although we expect to find mostly magnetic scattering at (2,2,0) and phonon scattering at (4,0,0), the finite Fe^{3+} magnetic form factor of $|F(\mathbf{Q})|$ means that there are still magnetic contributions to the phonon scattering at (4,0,0) $[|F(2,2,0)|^2/|F(4,0,0)|^2 \approx 1.86]$.

Magnetic neutron scattering directly measures the magnetic scattering function $S(\mathbf{Q},E)$, which is proportional to the imaginary part of the dynamic susceptibility $\chi''(\mathbf{Q},E)$ through $S(\mathbf{Q},E) \propto |F(\mathbf{Q})|^2\chi''(\mathbf{Q},E)/[1 - \exp(-\frac{E}{k_BT})]$, where E is the magnon energy, and k_B is the Boltzmann constant [2]. Although YIG is a ferrimagnet, its low-energy spin waves can be well described as a simple ferromagnet [17]. In the hydrodynamic limit of long wavelength (small q) and small energies, we expect $E = \Delta_0 + gH_0 + Dq^2$ for spin-wave dispersion, where Δ_0 is the possible intrinsic spin anisotropy gap, gH_0 is the size of the magnetic-field-induced spin gap, and

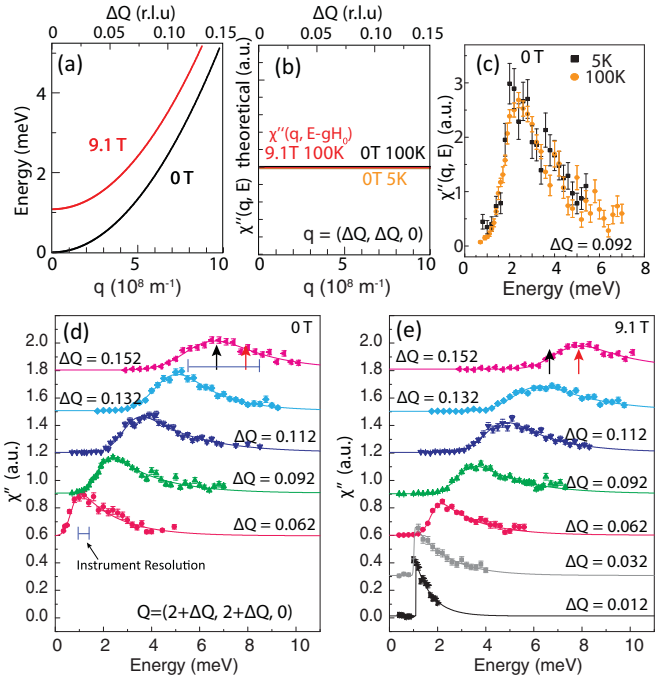

FIG. 2. (a) Schematic illustration of the expected magnon dispersions at 0 and 9.1 T for a simple ferromagnet. (b) The expected temperature, magnetic field dependence of low-energy $\chi''(\mathbf{Q},E)$ for a simple ferromagnet obtained from SPINW software package [39]. Here, the magnetic-field-induced spin gap gH_0 has been subtracted in the 9.1 T $\chi''(q,E-gH_0)$ (red). The upper and bottom units are ΔQ and q, respectively. (c) Our estimated $\chi''(\mathbf{Q},E)$ with $\mathbf{Q}=(2.092,2.092,0)$ at 5 and 100 K after correcting the measured $S(\mathbf{Q},E)$ for the background and Bose-population factor. (d), (e) The estimated $\chi''(\mathbf{Q},E)$ at 0 and 9.1 T, respectively, after correcting for background and Bose-population factor. Scans at different wave vectors are lifted up by 0.3 sequentially. The black and red arrows mark the peak positions at 0 and 9.1 T, respectively. The vertical error bars represent standard statistical errors throughout the paper.

D is in units of meV Å^2 [Fig. 2(a)] [13–16]. In addition, for a pure magnetic ordered system without spin-lattice interactions, we expect $\chi''(\mathbf{Q},E)$ to be independent of temperature at temperatures well below the magnetic ordering temperature and applied magnetic field after correcting for the field-induced spin gap gH_0 [Fig. 2(b)] [37–39].

To determine if the temperature and magnetic field dependence of spin waves in YIG follow these expectations, we measured the wave-vector dependence of magnon energy of YIG at different temperatures and magnetic fields. Figure 2(c) shows our estimated constant-$\mathbf{Q}$ scans [$\mathbf{Q}=(2.092,2.092,0)$ or $\Delta Q=0.092$ reciprocal-lattice units (r.l.u.)] of $\chi''(\mathbf{Q},E)$ at 5 K (solid black squares) and 100 K (solid orange circles). Consistent with the expectation, we see that $\chi''(\mathbf{Q},E)$ at these two temperatures are identical within the errors of the measurement. Figure 2(d) shows constant-$\mathbf{Q}$ scans of spin waves of YIG at 100 K and 0 T. At $\mathbf{Q}=(2.062,2.062,0)$ or $\Delta Q=0.062$, $\chi''(\mathbf{Q},E)$ has a clear peak in energy that is slightly larger than the instrumentation resolution (horizontal bar). With increasing ΔQ, the peak in $\chi''(\mathbf{Q},E)$ moves progressively to higher energies. We have attempted but failed to fit the spin-wave spectra with a simple harmonic oscillator generally used for a ferromagnet [38]. This may be consistent with a recent inelastic neutron scattering study of YIG that reveals the need to use long-range magnetic exchange couplings to fit the overall spin-wave spectra [19]. By fitting the spin-wave spectra at zero field with an exponentially modified Gaussian peak function [32], we obtain the magnon dispersion curve as shown in Fig. 1(e). Fitting the dispersion curve with $E=\Delta_0+Dq^2$ yields $\Delta_0\approx 0$ and $D=580\pm 60$ meV Å^2, consistent with earlier work giving $D\approx 533$ meV Å^2 [14].

Upon application of a 9.1 T field at 100 K, we expect the magnon dispersion curve to be lifted by $gH_0\approx 1$ meV. This would be consistent with the observation of a sharp gap below 1.05 meV in the constant-$\mathbf{Q}$ scan at $\mathbf{Q}=(2.012,2.012,0)$ ($\Delta Q=0.012$) [Fig. 2(e)]. The constant-$\mathbf{Q}$ scan at $\mathbf{Q}=(2.032,2.032,0)$ shows similar behavior. Figure 2(e) also shows constant-$\mathbf{Q}$ scans at wave vectors identical to those in Fig. 2(d) at 0 T. Using the data in Fig. 2(e), we plot the magnon dispersion at the 9.1 T field in Fig. 1(e). Consistent with the expectation, we see a clear gH_0 upward shift in magnon energy but the spin-wave stiffness D remains unchanged.

To quantitatively determine the magnetic field effect on $\chi''(\mathbf{Q},E)$ of YIG, we compare $\chi''(\mathbf{Q},E)$ at 0 T with those at 9.1 T. Figures 3(a)–3(d) summarize the energy dependence of $\chi''(\mathbf{Q},E)$ after downshifting the 9.1 T data by $gH_0=1.05$ meV. At $\Delta Q=0.062$, the scan along the red arrow direction near the magnon-phonon crossing point as shown in Fig. 1(f), we see that $\chi''(\mathbf{Q},E)$ at the 9.1 T field is lower in intensity compared with those at 0 T. On moving to $\Delta Q=0.10$ with no magnon-phonon crossing, the $\chi''(\mathbf{Q},E)$ at 0 and 9.1 T are virtually identical, as expected. At the second magnon-phonon crossing point with $\Delta Q\approx 0.13$ [see the red arrow in Fig. 1(g)], the differences between $\chi''(\mathbf{Q},E)$ at 0 and

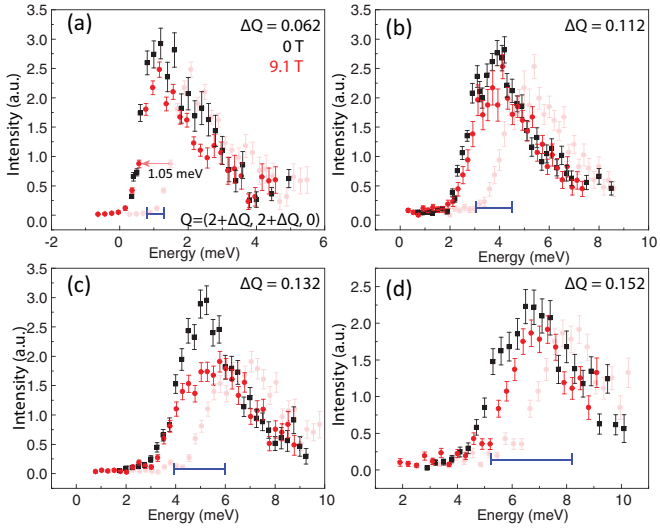

FIG. 3. (a)–(d) Comparison of the estimated $\chi''(\mathbf{Q},E)$ as a function of increasing wave vector at 0 T (black) and 9.1 T (red). The 9.1 T data are shifted by 1.05 meV to accommodate the field-induced energy shift. Light red dots represent the original data positions of the 9.1 T data. The horizontal bars are estimated instrumental energy resolutions based on magnon dispersion at 100 K.

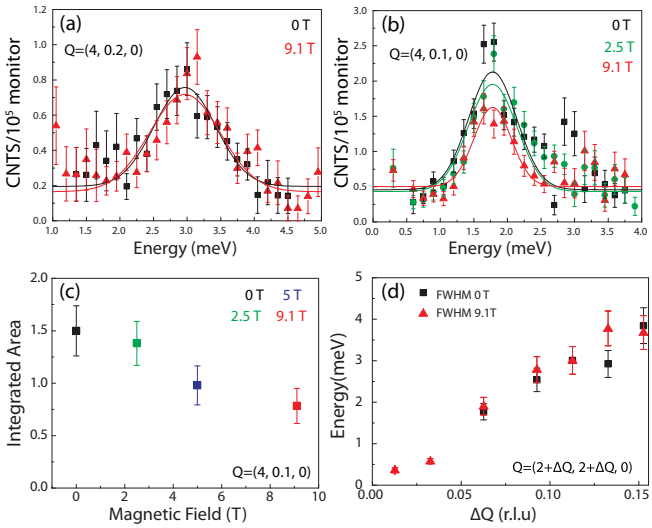

FIG. 4. (a) Energy scan of $S(\mathbf{Q},E)$ at $\mathbf{Q}=(4,0.2,0)$, a position far away from the magnon-phonon crossing points, and a temperature of 100 K to probe TA phonons at 0 and 9.1 T. (b) Energy scan of $S(\mathbf{Q},E)$ to probe magnon-phonon hybridized excitations at $\mathbf{Q}=(4,0.1,0)$ near the magnon-phonon crossing point at 0, 2.5, and 9.1 T. (c) Magnetic field dependence of the integrated intensity of magnon-phonon hybridized excitations at 100 K and $\mathbf{Q}=(4,0.1,0)$. (d) FWHM of the magnon at 0 and 9.1 T as a function of ΔQ.

9.1 T are even more obvious, with intensity at 0 T considerably larger than that at 9.1 T [Fig. 3(c)]. Finally, on moving to $\Delta Q=0.152$ well above the magnon-phonon crossing point wave vectors [Fig. 1(e)], we again see no obvious difference in $\chi''(\mathbf{Q},E)$ between 0 and 9.1 T.

Figure 3 shows that magnetic field dependence of $\chi''(\mathbf{Q},E)$ is highly wave-vector selective, revealing a clear magnetic-field-induced intensity reduction in $\chi''(\mathbf{Q},E)$ at wave vectors associated with magnon-phonon crossing points while having no effect at other wave vectors. To confirm the presence of a TA phonon and determine its magnetic field effect, we carried out TA phonon measurements near (4,0,0), which has a rather large nuclear structure factor compared with (2,2,0). Figure 4(a) shows the energy scans at $\mathbf{Q}=(4,0.2,0)$ and 100 K, which are along the green arrow direction in Fig. 1(g) and far away from the magnon dispersion. The spectra reveal a clear magnetic-field-independent peak at $E\approx 3$ meV, confirming the TA phonon nature of the scattering. Figure 4(b) shows a similar energy scan at $\mathbf{Q}=(4,0.1,0)$ and 100 K, which is along the green arrow direction and near the magnon-phonon crossing point in Fig. 1(f). At 0 T, we see a peak around $E\approx 1.7$ meV, consistent with dispersions of magnons and TA phonons. With increasing field to 2.5 and 9.1 T, the intensity of the peak decreases, but its position in energy remains unchanged [Fig. 4(b)]. Figure 4(c) shows the magnetic field dependence of the integrated intensity, confirming the results in Fig. 4(b). Since the energy of the magnon should increase with increasing magnetic field, the field-independent nature of the peak position in Fig. 4(b) suggests that the mode cannot be a simple addition of a magnon and phonon, but most likely arises from hybridized magnon polarons [6,7]. Figure 4(d) shows the full width at half maximum (FWHM) of the magnon width at 0 and 9.1 T. Within the errors of our measurements, we see no energy width change in the measured wave-vector region.

Our results provided compelling evidence for the presence of magnon-phonon coupling in YIG at the magnon-phonon crossing points at zero field. This is clearly different from the SSE measurements, where anomalies are only seen at the critical fields that obey a "touch" condition at which the magnon energy and group velocity agree with those of the TA/LA phonons. When the applied field is less than the critical field, the magnon dispersion has two intersections with the TA/LA phonon modes. When the applied field is larger than the critical field, the magnon dispersoin is separated from the TA/LA phonon modes. In the theory of hybrid magnon-phonon excitations [6,7], SSE anomalies occur at magnetic fields and wave vectors at which the phonon dispersion curves are tangents to the magnon dispersion, where the effects of magnon-phonon coupling are maximized [40]. While our findings of a different magnon-phonon coupling at zero field are consistent with the formation of magnon polarons in YIG [6,7], they are not direct proof that magnon-polaron formation alone causes anomalous features in the magnetic field and temperature dependence of the SSE. Other effects, such as spin diffusion length, the acoustic quality of the YIG film, and magnon spin conductivity also play an important role in determining the SSE anomaly [41]. Regardless of the microscopic origin of the SSE anomaly, our discovery suggests the need to understand why magnon-phonon interactions and the resulting magnon polarons enhance the hybridized excitations at the magnon-phonon intersection points.

The neutron scattering work at Rice is supported by the U.S. DOE, BES DE-SC0012311 (P.D.). The materials work at Rice is supported by the Robert A. Welch Foundation Grant No. C-1839 (P.D.). The work at UCR (J.S. and Z.S.) is supported as part of the SHINES, an Energy Frontier Research Center funded by the U.S. DOE, BES under Award No. SC0012670. YIG crystal growth at UT-Austin is supported by the Army Research Office MURI Award No. W911NF-14-1-0016. The work at BNU (K.X.) is supported by NSFC (Grant No. 61774017).

H.M. and Z.S. contributed equally to this work.

[1] W. Heisenberg, Z. Phys. **49**, 619 (1928).

[2] S. W. Lovesey, *Theory of Thermal Neutron Scattering from Condensed Matter* (Clarendon, Oxford, UK, 1984), Vol. 2, Chap. 9.

[3] L. D. Landau, Sov. Phys. JETP **3**, 920 (1957).

[4] M. E. Zhitomirsky and A. L. Chernyshev, Rev. Mod. Phys. **85**, 219 (2013).

[5] J. Zhao, D. T. Adroja, D.-X. Yao, R. Bewley, S. Li, X. F. Wang, G. Wu, X. H. Chen, J. Hu, and P. Dai, Nat. Phys. **5**, 555 (2009).

[6] A. Kamra, H. Keshtgar, P. Yan, and G. E. W. Bauer, Phys. Rev. B **91**, 104409 (2015).
[7] K. Shen and G. E. W. Bauer, Phys. Rev. Lett. **115**, 197201 (2015).
[8] E. Anda, J. Phys. C **9**, 1075 (1976).
[9] S. C. Guerreiro and S. M. Rezende, Phys. Rev. B **92**, 214437 (2015).
[10] J. Oh, M. D. Le, H.-H. Nahm, H. Sim, J. Jeong, T. G. Perring, H. Woo, K. Nakajima, S. Ohira-Kawamura, Z. Yamani, Y. Yoshida, H. Eisaki, S.-W. Cheong, A. L. Chernyshev, and J.-G. Park, Nat. Commun. **7**, 13146 (2016).
[11] P. Dai, H. Y. Hwang, J. Zhang, J. A. Fernandez-Baca, S.-W. Cheong, C. Kloc, Y. Tomioka, and Y. Tokura, Phys. Rev. B **61**, 9553 (2000).
[12] S. Geller and M. A. Gilleo, Acta Crystallogr. **10**, 239 (1957).
[13] J. S. Plant, J. Phys. C **10**, 4805 (1977).
[14] V. Cherepanov, I. Kolokolov, and V. L'vov, Phys. Rep. **229**, 81 (1993).
[15] A. B. Harris, Phys. Rev. **132**, 2398 (1963).
[16] C. M. Srivastava and R. Aiyar, J. Phys. C **20**, 1119 (1987).
[17] J. Barker and G. E. W. Bauer, Phys. Rev. Lett. **117**, 217201 (2016).
[18] L. S. Xie, G. X. Jin, L. X. He, G. E. W. Bauer, J. Barker, and K. Xia, Phys. Rev. B **95**, 014423 (2017).
[19] A. J. Princep, R. A. Ewings, S. Ward, S. Tóth, C. Dubs, D. Prabhakaran, and A. T. Boothroyd, arXiv:1705.06594.
[20] T. Kikkawa, K. Shen, B. Flebus, R. A. Duine, K.-i. Uchida, Z. Qiu, G. E. W. Bauer, and E. Saitoh, Phys. Rev. Lett. **117**, 207203 (2016).
[21] A. V. Chumak, V. I. Vasyuchka, A. A. Serga, and B. Hillebrands, Nat. Phys. **11**, 453 (2015).
[22] A. A. Serga, A. V. Chumak, and B. Hillebrands, J. Phys. D: Appl. Phys. **43**264002 (2010).
[23] A. V. Chumak, A. A. Serga, and B. Hillebrands, Nat. Commun. **5**, 4700 (2014).
[24] Y. Kajiwara, K. Harii, S. Takahashi, J. Ohe, K. Uchida, M. Mizuguchi, H. Umezawa, H. Kawai, K. Ando, K. Takanashi, S. Maekawa, and E. Saitoh, Nature (London) **464**, 262 (2010).
[25] G. E. W. Bauer, E. Saitoh, and B. J. van Wees, Nat. Mater. **11**, 391 (2012).
[26] K. Uchida, S. Takahashi, K. Harii, J. Ieda, W. Koshibae, K. Ando, S. Maekawa, and E. Saitoh, Nature (London) **455**, 778 (2008).
[27] K. Uchida, J. Xiao, H. Adachi, J. Ohe, S. Takahashi, J. Ieda, T. Ota, Y. Kajiwara, H. Umezawa, H. Kawai, G. E. W. Bauer, S. Maekawa, and E. Saitoh, Nat. Mater. **9**, 894 (2010).
[28] H. Adachi, K.-i. Uchida, E. Saitoh, J.-i. Ohe, S. Takahashi, and S. Maekawa, Appl. Phys. Lett. **97**, 252506 (2010).
[29] C. M. Jaworski, J. Yang, S. Mack, D. D. Awschalom, R. C. Myers, and J. P. Heremans, Phys. Rev. Lett. **106**, 186601 (2011).
[30] A. Hoffmann and S. D. Bader, Phys. Rev. Appl. **4**, 047001 (2015).
[31] Y. Hashimoto, S. Daimon, R. Iguchi, Y. Oikawa, K. Shen, K. Sato, D. Bossini, Y. Tabuchi, T. Satoh, B. Hillebrands, G. E. W. Bauer, T. H. Johansen, A. Kirilyuk, T. Rasing, and E. Saitoh, Nat. Comm. **8**, 15859 (2017).
[32] See Supplemental Material at http://link.aps.org/supplemental/10.1103/PhysRevB.96.100406 for additional data and analysis, which includes Ref. [42].
[33] Z. Jiang, C.-Z. Chang, M. R. Masir, C. Tang, Y. Xu, J. S. Moodera, A. H. MacDonald, and J. Shi, Nat. Commun. **7**, 11458 (2016).
[34] Y. D. Xu, B. Yang, C. Tang, Z. Jiang, M. Schneider, R. Whig, and J. Shi, Appl. Phys. Lett. **105**, 242404 (2014).
[35] S. M. Wu, F. Y. Fradin, J. Hoffman, A. Hoffmann, and A. Bhattacharya, J. Appl. Phys. **117**, 17C509 (2015).
[36] M. Collet, L. Soumah, P. Bortolotti, M. Muñoz, V. Cros, and A. Anane, AIP Adv. **7**, 055924 (2017).
[37] P. Dai, Rev. Mod. Phys. **87**, 855 (2015).
[38] F. Ye, P. C. Dai, J. A. Fernandez-Baca, D. T. Adroja, T. G. Perring, Y. Tomioka, and Y. Tokura, Phys. Rev. B **75**, 144408 (2007).
[39] S. Toth and B. Lake, J. Phys.: Condens. Matter **27**, 166002 (2015).
[40] B. Flebus, K. Shen, T. Kikkawa, K.-i. Uchida, Z. Qiu, E. Saitoh, R. A. Duine, and G. E. W. Bauer, Phys. Rev. B **95**, 144420 (2017).
[41] L. J. Cornelissen, K. Oyanagi, T. Kikkawa, Z. Qiu, T. Kuschel, G. E. W. Bauer, B. J. van Wees, and E. Saitoh, arXiv:1706.04373.
[42] S. Kimura and I. Shindo, J. Cryst. Growth **41**, 192 (1977).